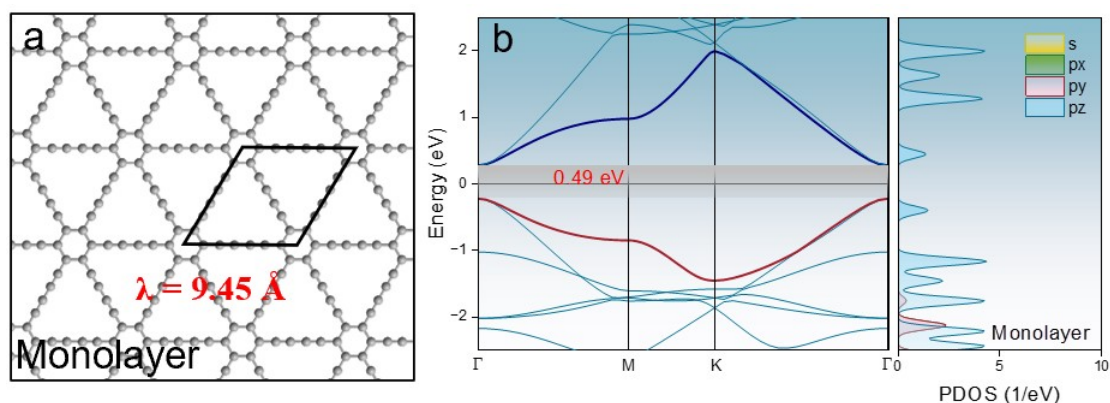


## Supporting Information

### Enhanced Thermoelectric Properties in Bilayer Graphdiyne through Twist Angle and Pressure

Qiaohan Liu,<sup>a</sup> Dapeng Wu<sup>\*,a</sup> and Jingang Wang<sup>\*,a</sup>

College of Science, Liaoning Petrochemical University, Fushun 113001, China



**Fig S1:** (a) Schematic diagram of the structure of monolayer graphdiyne (GDY) (where  $\lambda$  represents the lattice constant); (b) The band structure and projected density of states diagram in GDY.

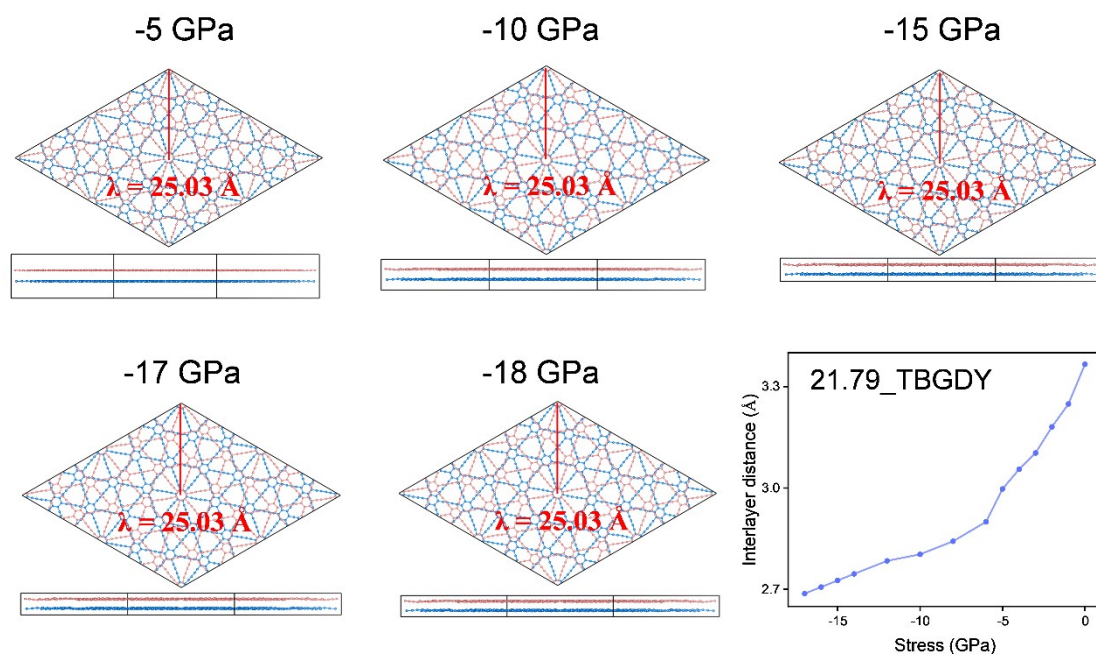


**Fig S2:** Schematic diagram of the 21.79°\_TBGDY structure under the compressive stress in the out-of-plane (Z direction). And the line chart of the change in interlayer spacing.

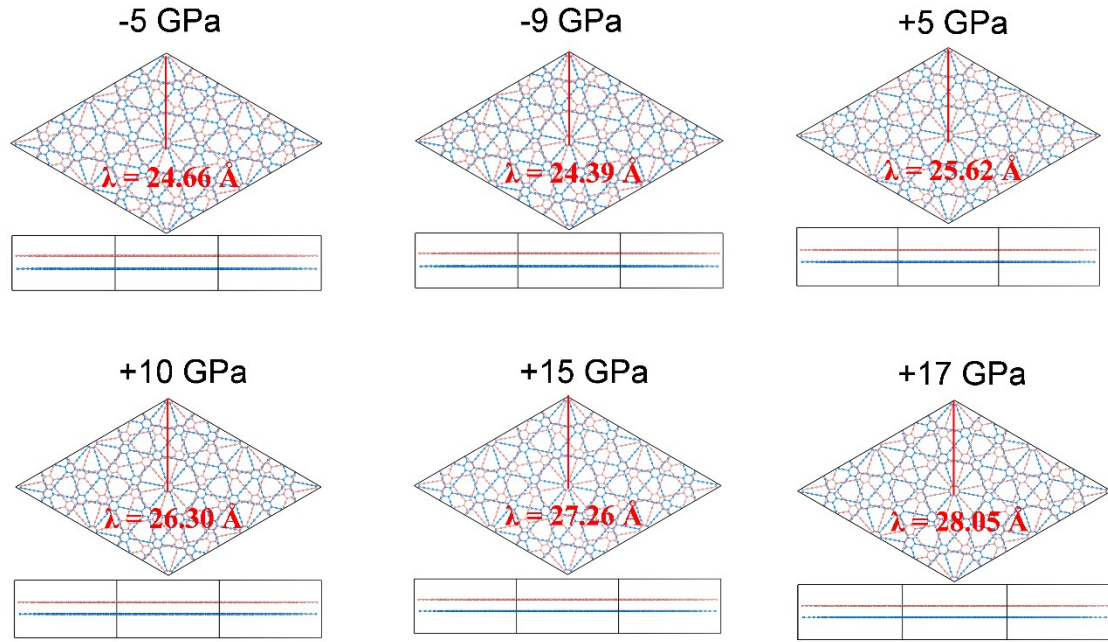


**Fig S3:** Schematic diagram of the 21.79°\_TBGDY structure under compressive and tensile stresses in the in-plane direction (XY direction). And the line chart of the change in interlayer spacing.

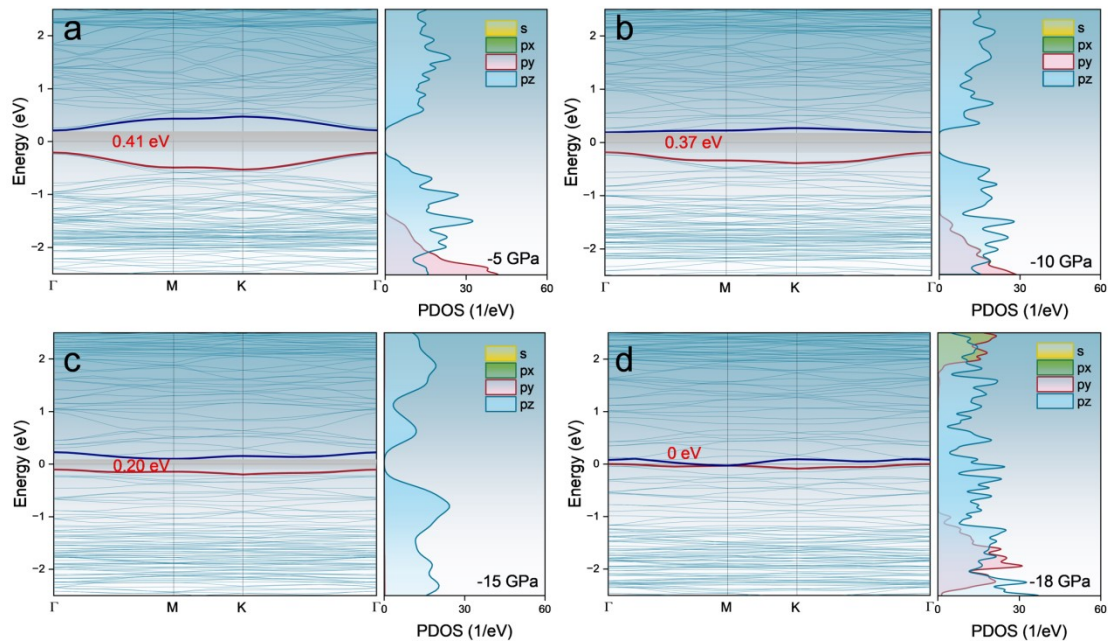


**Fig S4:** The band structure and projected density of states diagrams of the 21.79°\_TBGDY structure in the out-of-plane direction (Z direction): (a) Z\_-5 GPa; (b) Z\_-10 GPa; (c) Z\_-15 GPa; (d) Z\_-18 GPa.

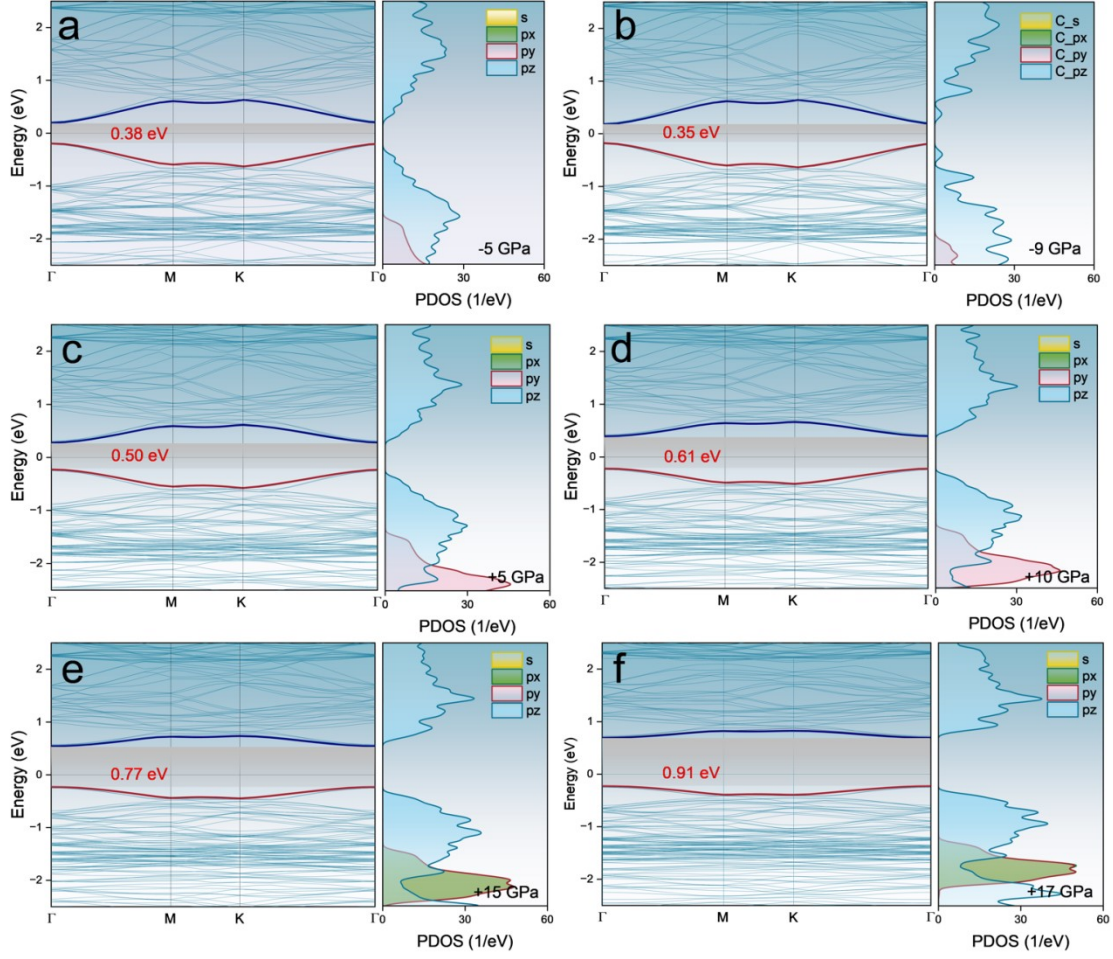


**Fig S5:** The band structure and projected density of states diagrams of the  $21.79^\circ$ \_TBGDY structure under the compressive stress in the in-plane direction (XY direction): (a) XY\_-5 GPa; (b) XY\_-9 GPa; (c) XY\_+5 GPa; (d) XY\_+10 GPa; (e) XY\_+15 GPa; (f) XY\_+17 GPa.

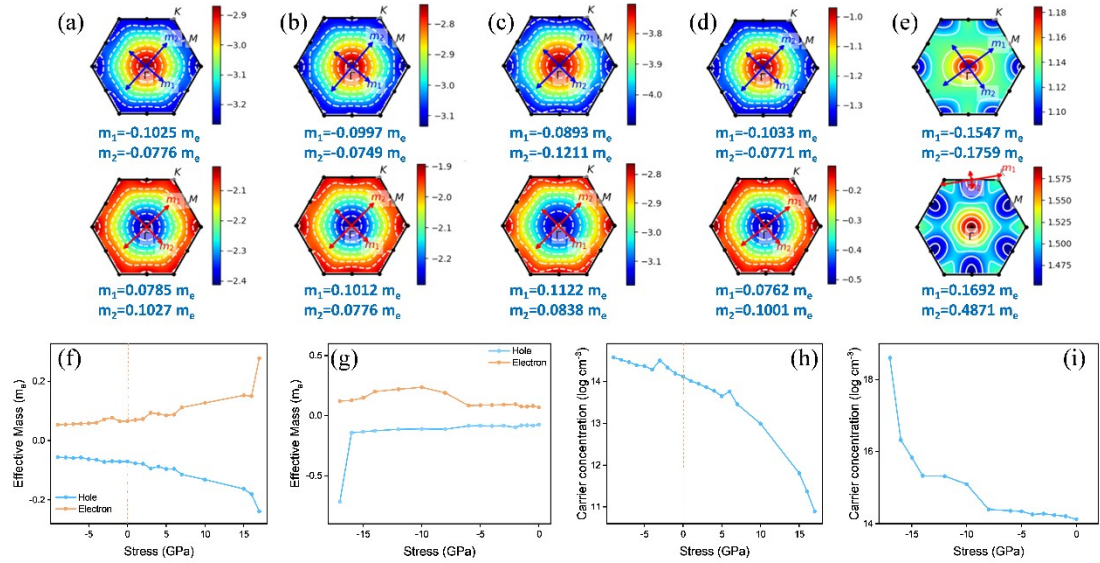


**Fig S6:** Color plots of the effective masses of holes (upper part) and electrons (lower part) within the first Brillouin zone of the  $21.79^\circ$ \_TBGDY structure under stresses in different directions. (a)  $21.79^\circ$ \_TBGDY without external stress; (b) XY\_-9 GPa; (c)

XY\_17 GPa; (d) Z\_-8 GPa; (e) Z\_-17 GPa. (f) Schematic diagram of the effective mass of  $21.79^\circ$ \_TBGDY with stress applied in the in-plane direction (XY direction); (g) Schematic diagram of the effective mass of  $21.79^\circ$ \_TBGDY with stress applied in the out-of-plane direction (Z direction); (h) Schematic diagram of the carrier concentration of  $21.79^\circ$ \_TBGDY with stress applied in the in-plane direction (XY direction) at 300K; (i) Schematic diagram of the carrier concentration of  $21.79^\circ$ \_TBGDY with stress applied in the out-of-plane direction (Z direction) at 300K.

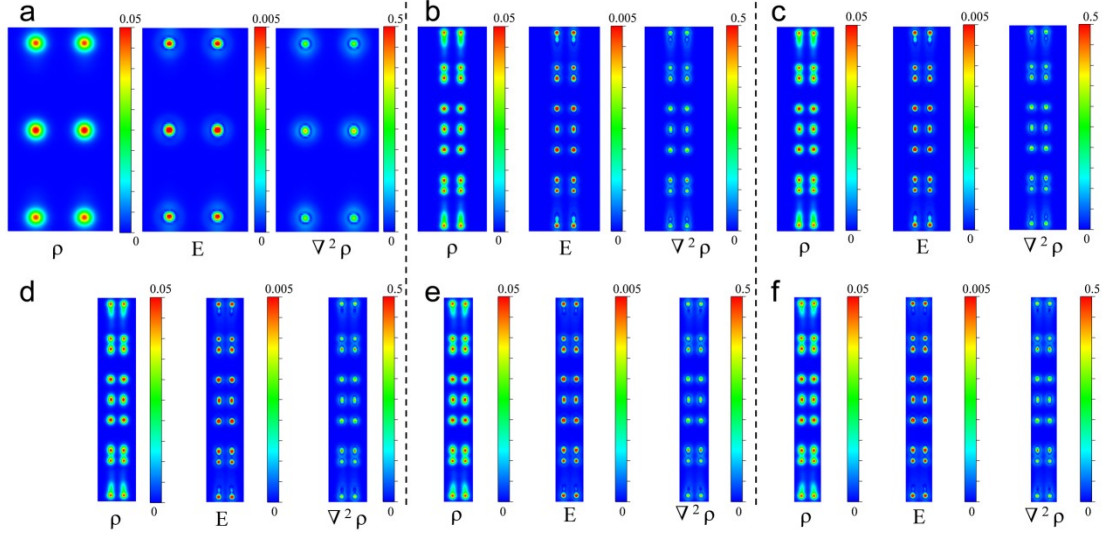


**Fig S7:** Intermolecular bonding characteristics of different structures: (a) Bilayer; (b)  $21.79^\circ$ \_TBGDY; (c) Z\_-5 GPa; (d) Z\_-10 GPa; (e) Z\_-15 GPa; (f) Z\_-18 GPa.

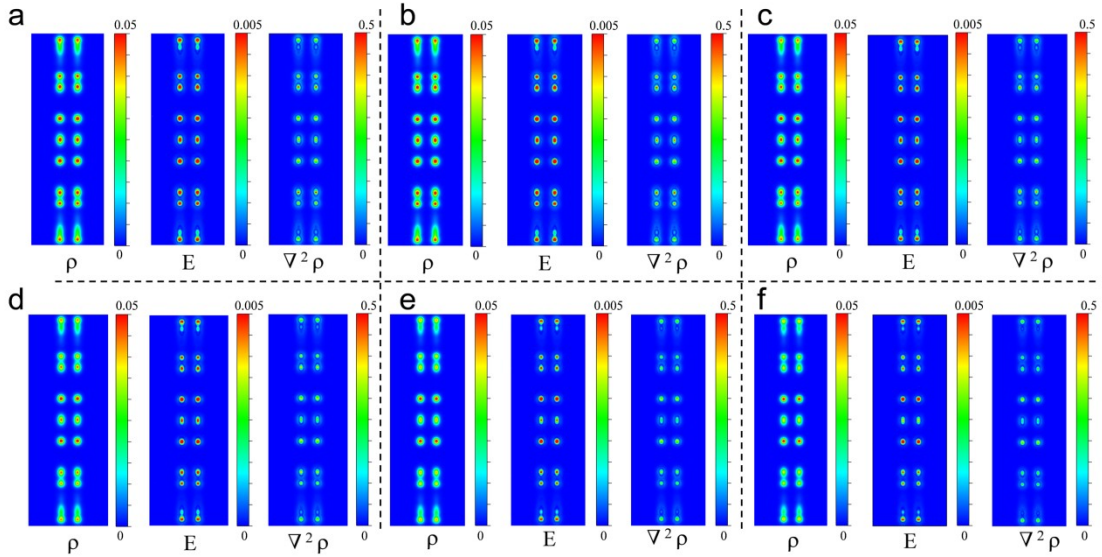


**Fig S8:** Intermolecular bonding characteristics of different structures: (a) XY\_-5 GPa; (b) XY\_-9 GPa; (c) XY\_+5 GPa; (d) XY\_+10 GPa; (e) XY\_+15 GPa; (f) XY\_+17 GPa.

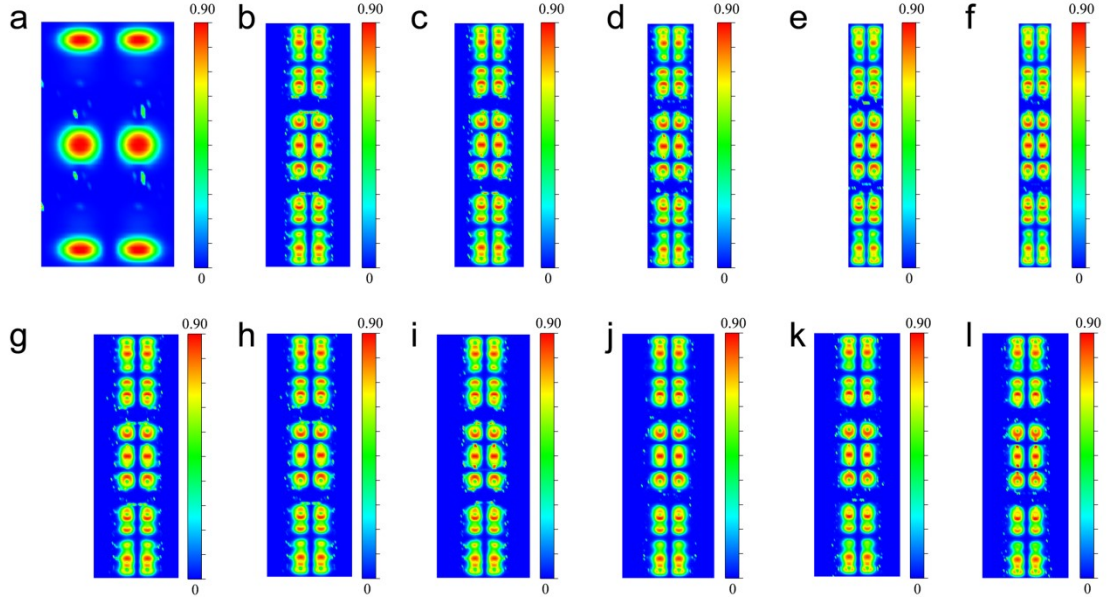


**Fig S9:** Electron localization functions of different structures: (a) Bilayer; (b) 21.79°\_TBGDY; (c) Z\_-5 GPa; (d) Z\_-10 GPa; (e) Z\_-15 GPa; (f) Z\_-18 GPa; (g) XY\_-5 GPa; (h) XY\_-9 GPa; (i) XY\_+5 GPa; (j) XY\_+10 GPa; (k) XY\_+15 GPa; (l) XY\_+17 GPa.

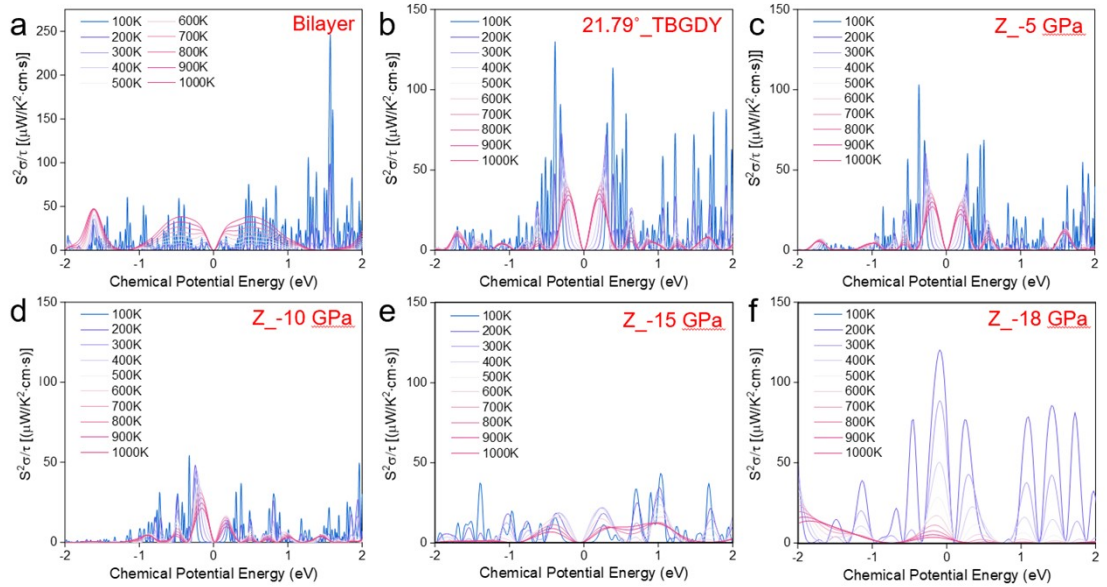


**Fig S10:** The chemical potential-dependent power factor at different temperatures: (a) Bilayer; (b) 21.79°\_TBGDY; (c) Z\_-5 GPa; (d) Z\_-10 GPa; (e) Z\_-15 GPa; (f) Z\_-18 GPa.

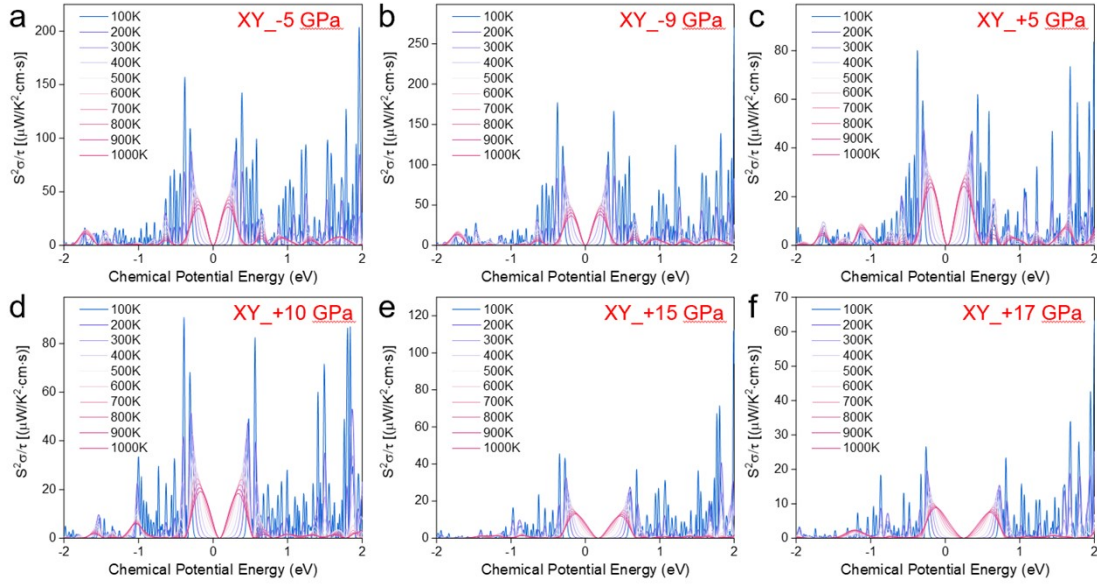


**Fig S11:** The power factor dependent on the chemical potential at different temperatures: (a) XY\_-5 GPa; (b) XY\_-9 GPa; (c) XY\_+5 GPa; (d) XY\_+10 GPa; (e) XY\_+15 GPa; (f) XY\_+17 GPa.

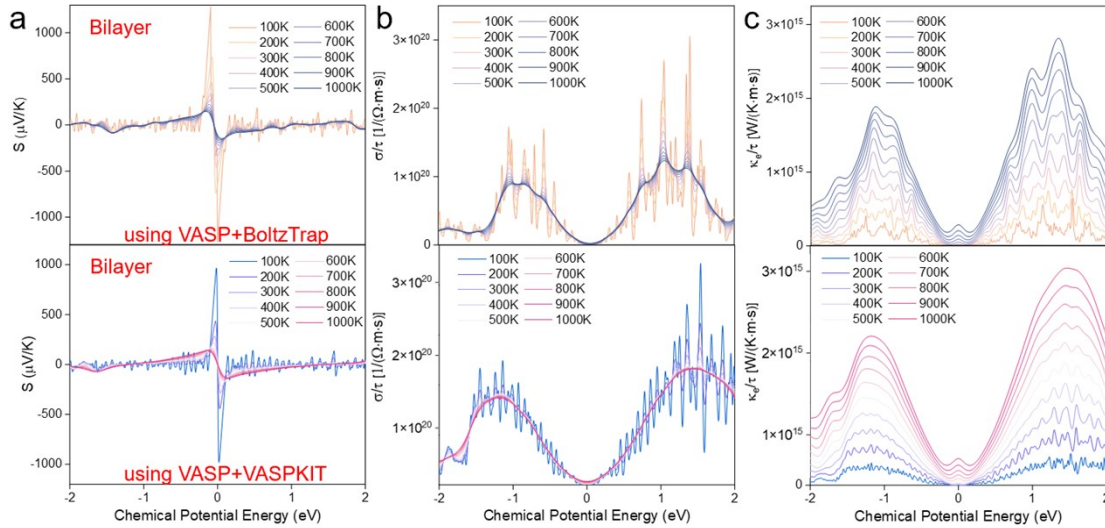


**Fig S12:** The chemical potential-dependent (a) Seebeck coefficient; (b) the ratios of electrical conductivity to the relaxation time ( $\sigma/\tau$ ); (c) the ratios of electronic thermal conductivity to the relaxation time ( $\kappa_e/\tau$ ) of the Bilayer structure at different temperatures (Two calculation methods: The upper one is the VASP + BoltzTrap method; the lower one is the VASP + VASPKIT method).

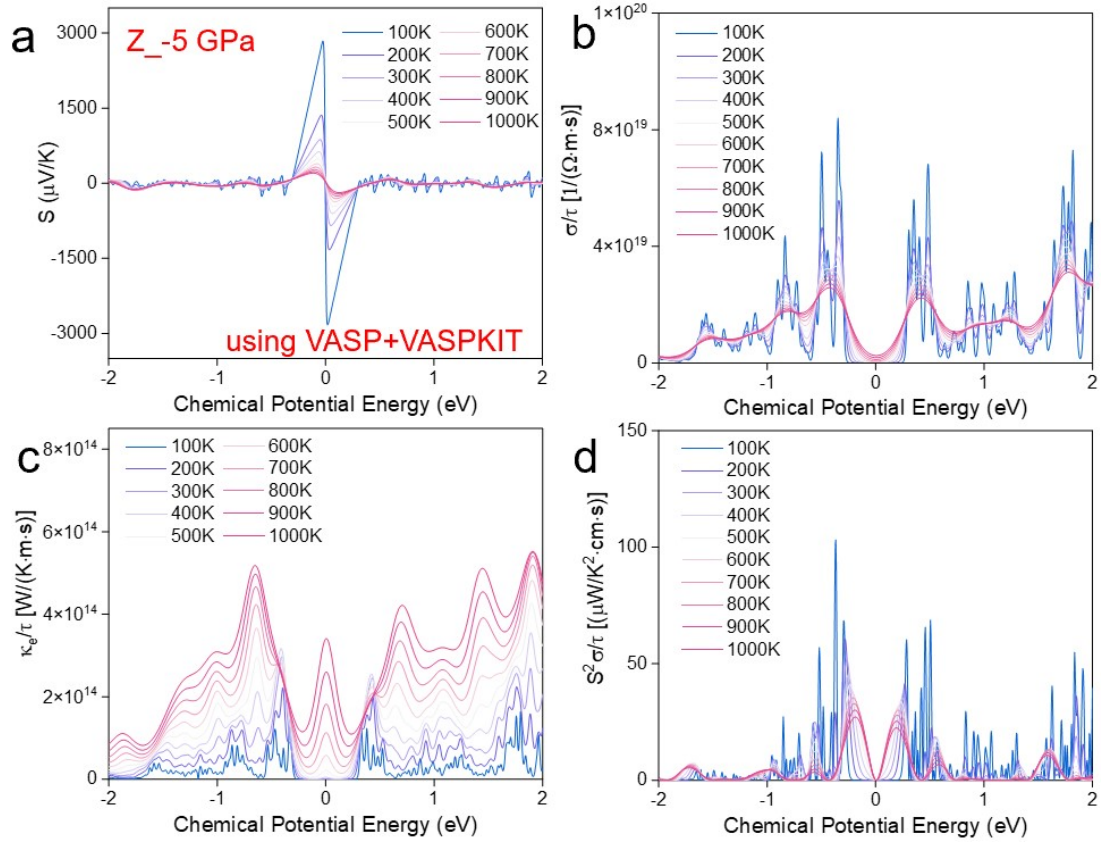


**Fig S13:** The chemical potential-dependent (a) Seebeck coefficient; (b) the ratios of electrical conductivity to the relaxation time ( $\sigma/\tau$ ); (c) the ratios of electronic thermal conductivity to the relaxation time ( $\kappa_e/\tau$ ); (d) the ratios of power factor to the relaxation time ( $PF/\tau$ ) of Z<sub>-5</sub> GPa at different temperatures.

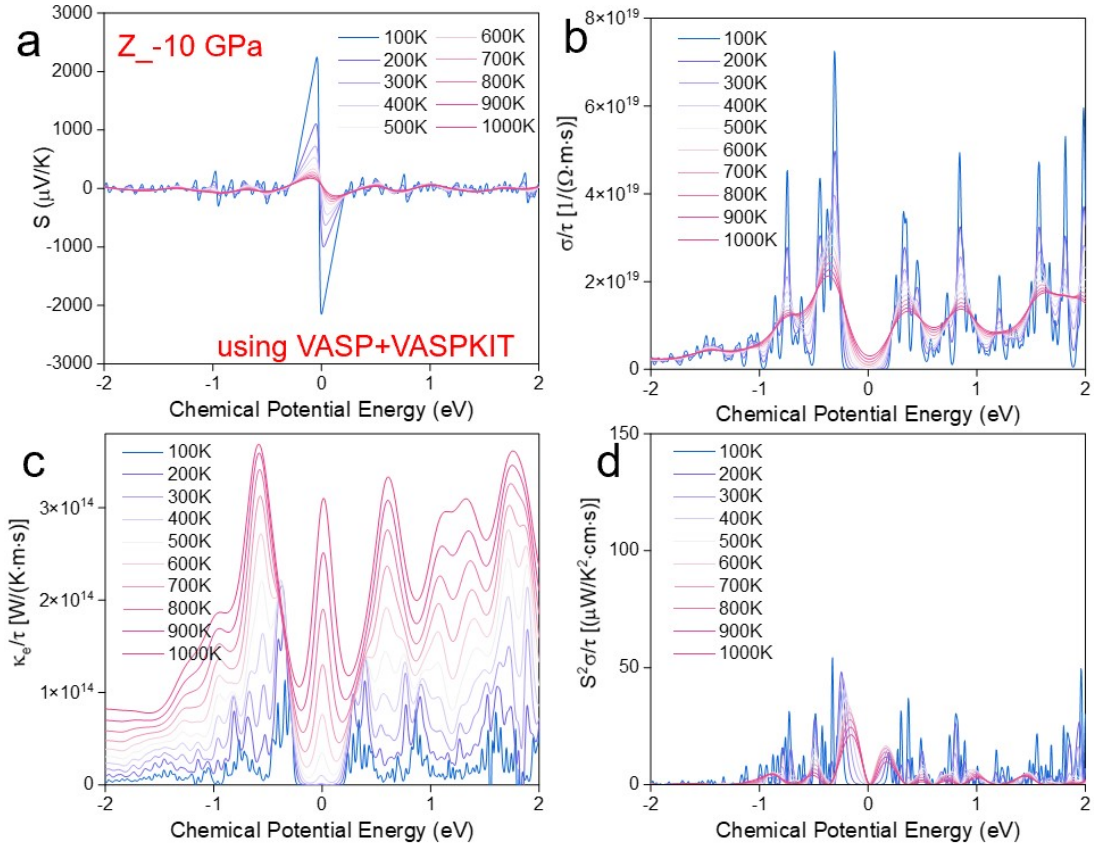


**Fig S14:** The chemical potential-dependent (a) Seebeck coefficient; (b) the ratios of electrical conductivity to the relaxation time ( $\sigma/\tau$ ); (c) the ratios of electronic thermal conductivity to the relaxation time ( $\kappa_e/\tau$ ); (d) the ratios of power factor to the relaxation time ( $PF/\tau$ ) of Z<sub>-10</sub> GPa at different temperatures.

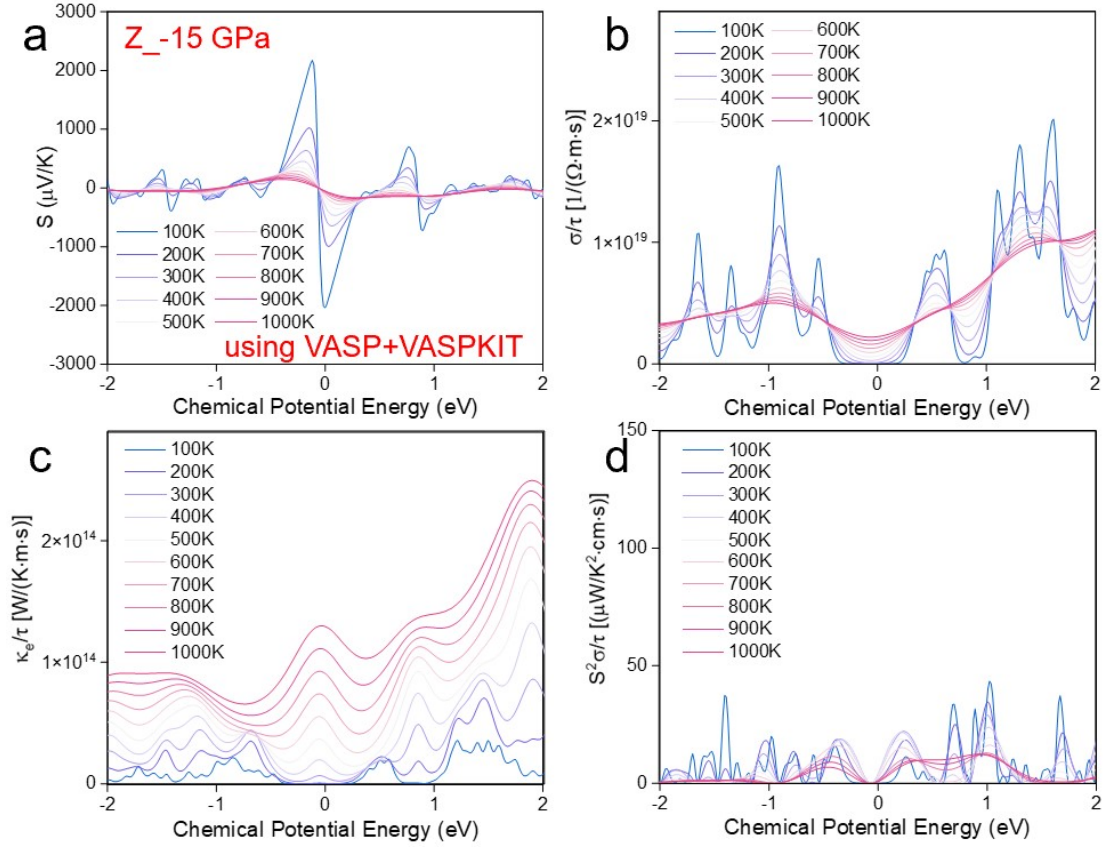


**Fig S15:** The chemical potential-dependent (a) Seebeck coefficient; (b) the ratios of electrical conductivity to the relaxation time ( $\sigma/\tau$ ); (c) the ratios of electronic thermal conductivity to the relaxation time ( $\kappa_e/\tau$ ); (d) the ratios of power factor to the relaxation time ( $PF/\tau$ ) of  $Z_{-15}$  GPa at different temperatures.

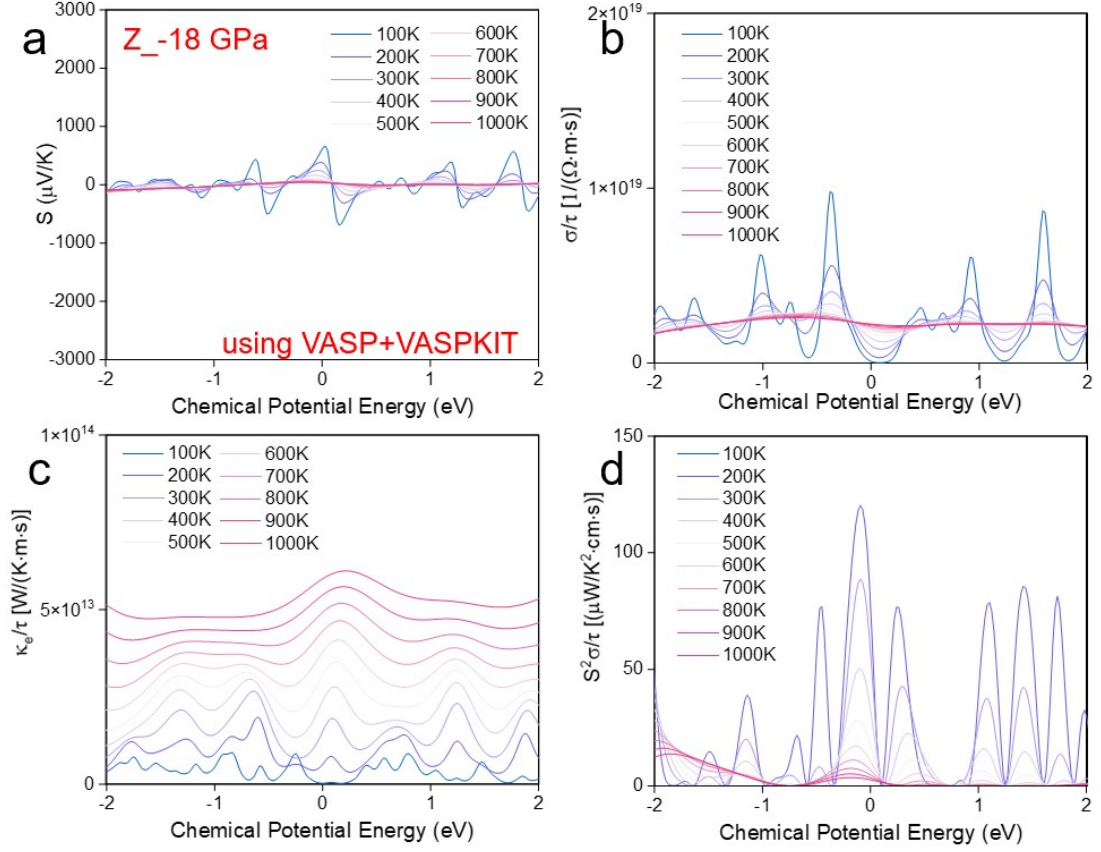


**Fig S16:** The chemical potential-dependent (a) Seebeck coefficient; (b) the ratios of electrical conductivity to the relaxation time ( $\sigma/\tau$ ); (c) the ratios of electronic thermal conductivity to the relaxation time ( $\kappa_e/\tau$ ); (d) the ratios of power factor to the relaxation time ( $PF/\tau$ ) of Z<sub>-</sub>18 GPa at different temperatures.

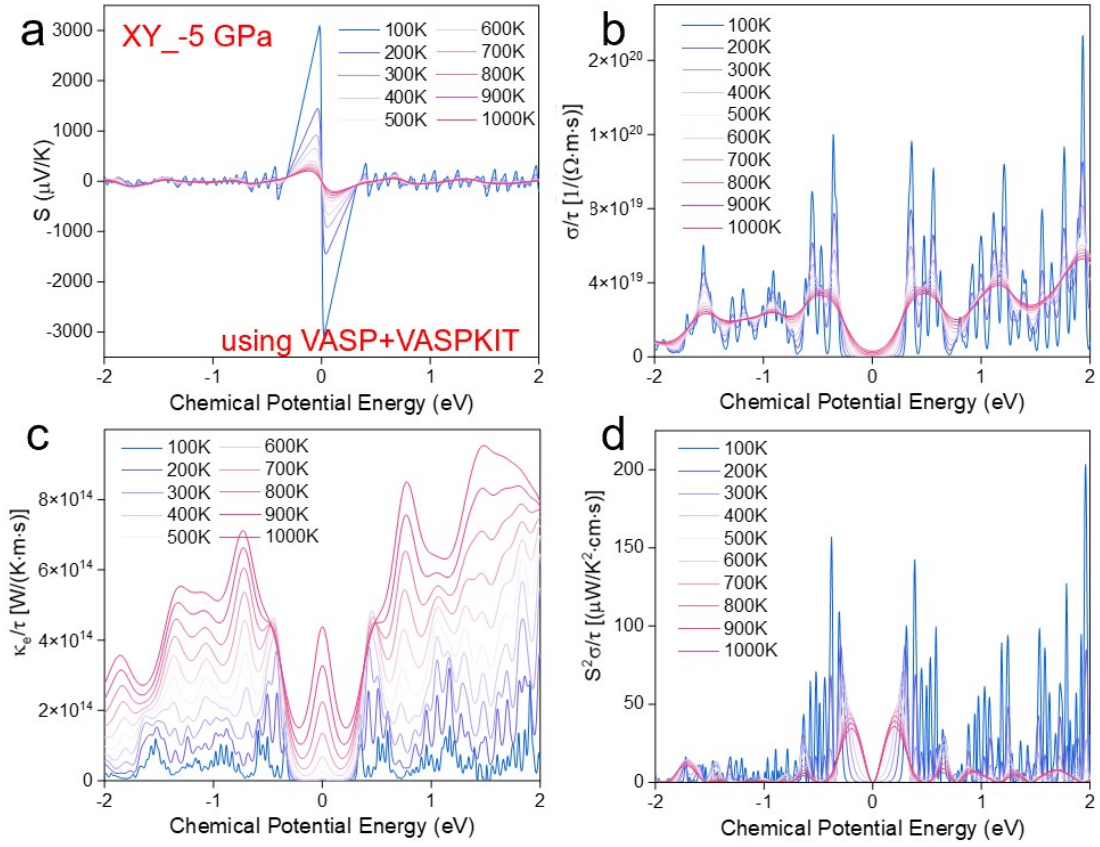


**Fig S17:** The chemical potential-dependent (a) Seebeck coefficient; (b) the ratios of electrical conductivity to the relaxation time ( $\sigma/\tau$ ); (c) the ratios of electronic thermal conductivity to the relaxation time ( $\kappa_e/\tau$ ); (d) the ratios of power factor to the relaxation time ( $PF/\tau$ ) of XY<sub>-5</sub> GPa at different temperatures.

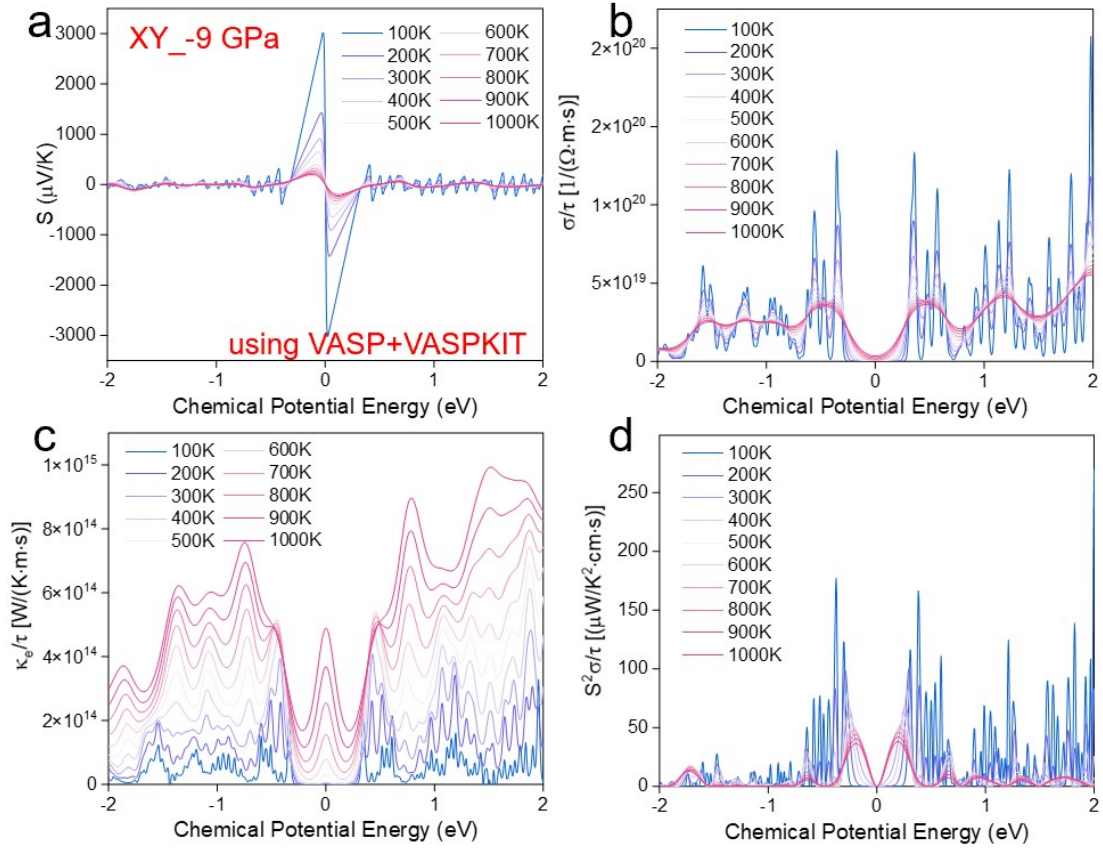


**Fig S18:** The chemical potential-dependent (a) Seebeck coefficient; (b) the ratios of electrical conductivity to the relaxation time ( $\sigma/\tau$ ); (c) the ratios of electronic thermal conductivity to the relaxation time ( $\kappa_e/\tau$ ); (d) the ratios of power factor to the relaxation time ( $PF/\tau$ ) of XY<sub>-9</sub> GPa at different temperatures.

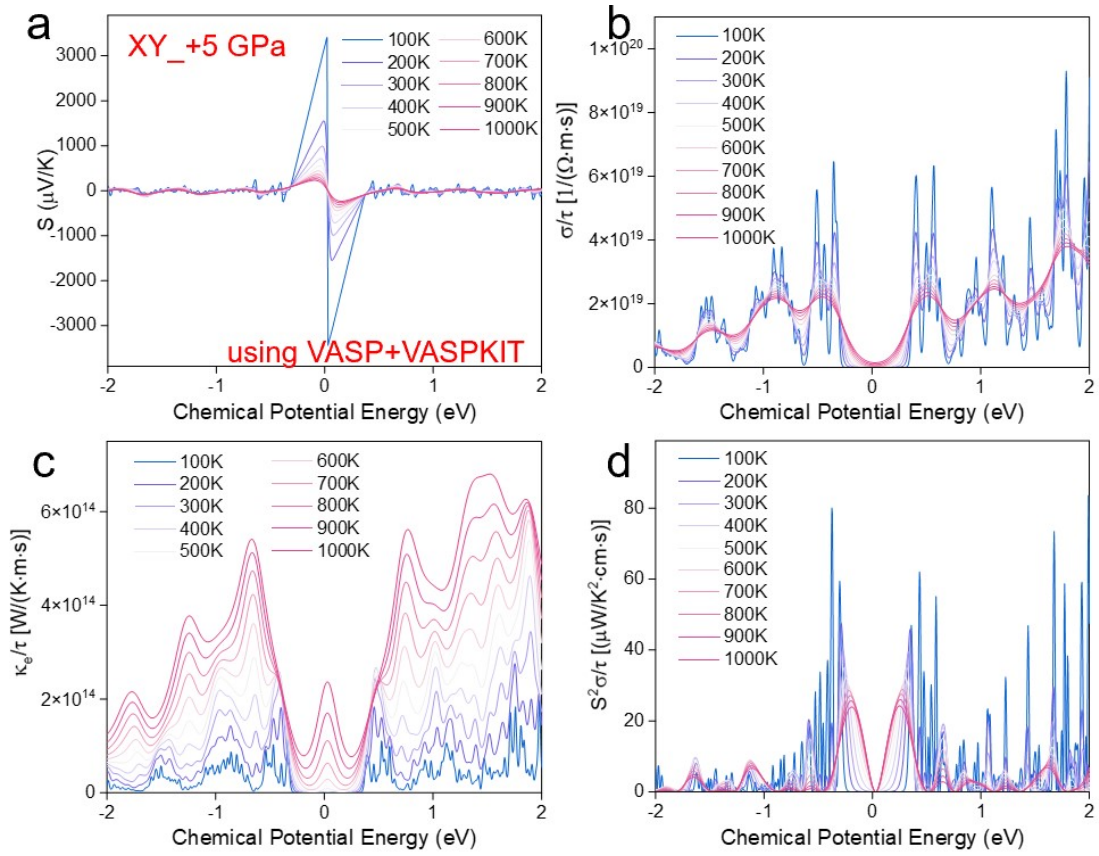


**Fig S19:** The chemical potential-dependent (a) Seebeck coefficient; (b) the ratios of electrical conductivity to the relaxation time ( $\sigma/\tau$ ); (c) the ratios of electronic thermal conductivity to the relaxation time ( $\kappa_e/\tau$ ); (d) the ratios of power factor to the relaxation time ( $PF/\tau$ ) of XY<sub>+</sub>5 GPa at different temperatures.

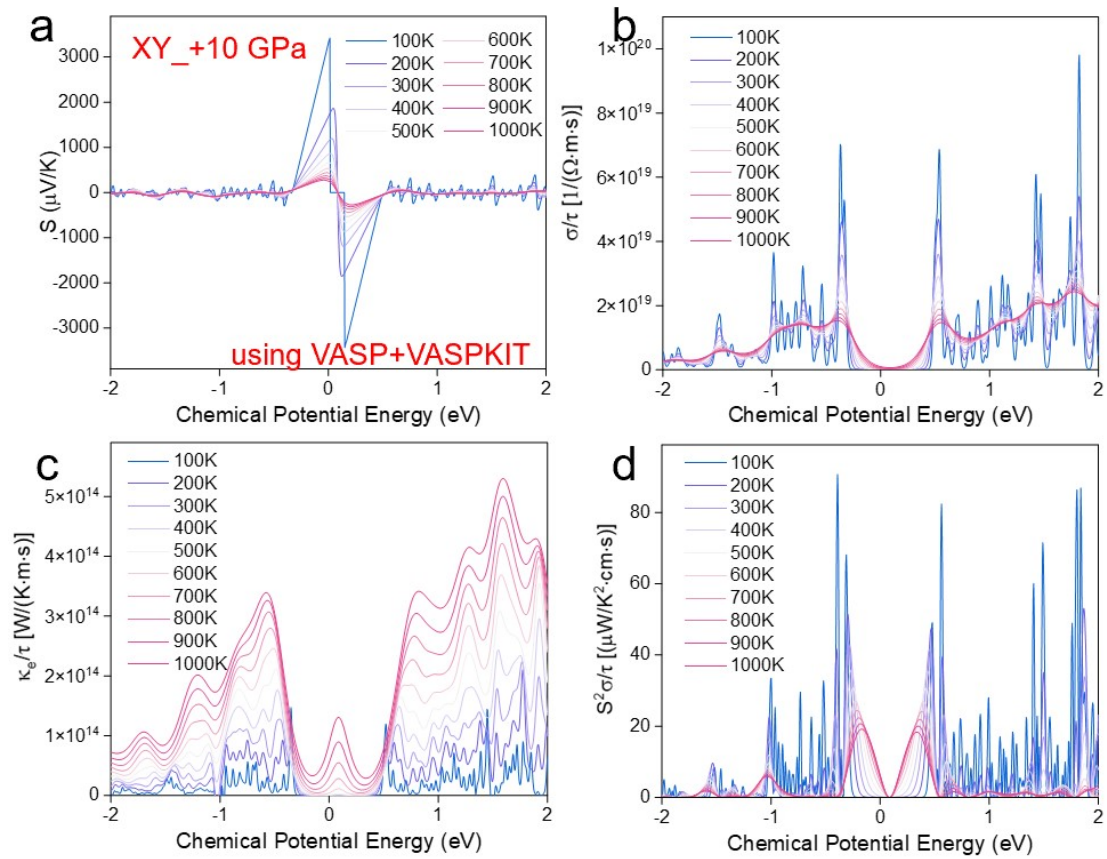


**Fig S20:** The chemical potential-dependent (a) Seebeck coefficient; (b) the ratios of electrical conductivity to the relaxation time ( $\sigma/\tau$ ); (c) the ratios of electronic thermal conductivity to the relaxation time ( $\kappa_e/\tau$ ); (d) the ratios of power factor to the relaxation time ( $PF/\tau$ ) of XY<sub>+</sub>+10 GPa at different temperatures.

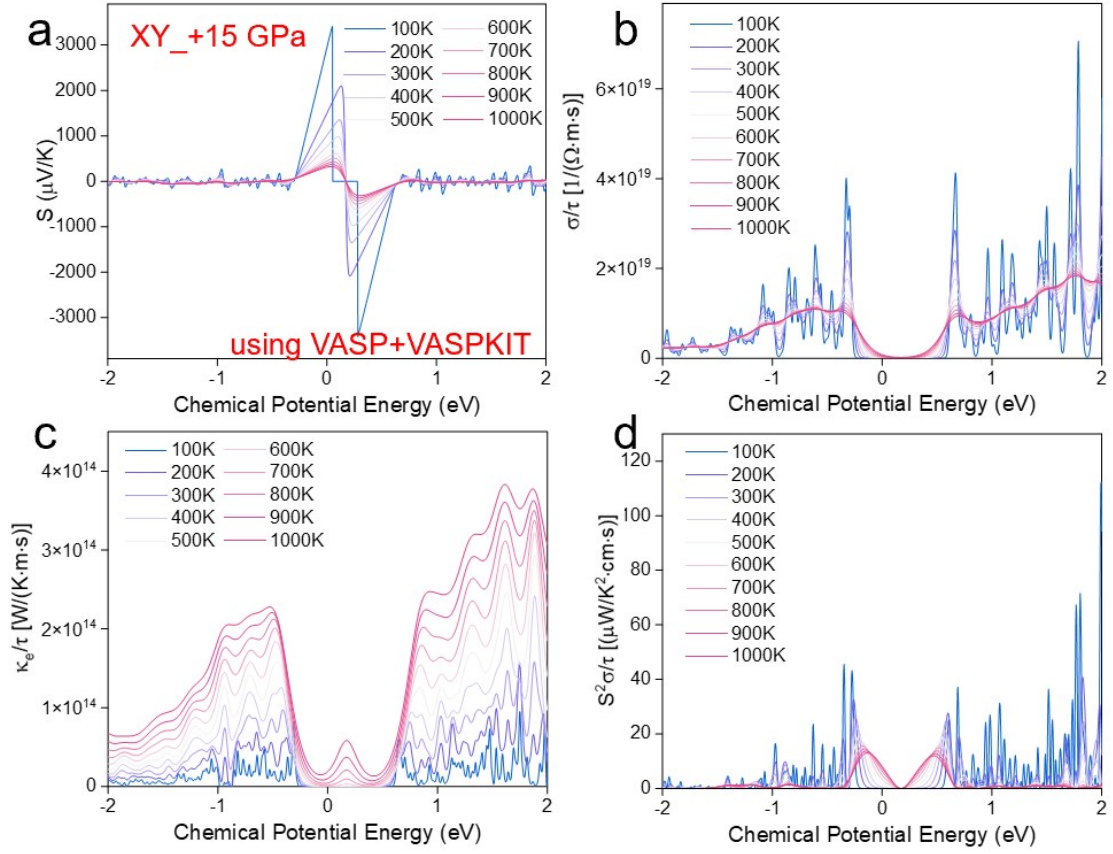


**Fig S21:** The chemical potential-dependent (a) Seebeck coefficient; (b) the ratios of electrical conductivity to the relaxation time ( $\sigma/\tau$ ); (c) the ratios of electronic thermal conductivity to the relaxation time ( $\kappa_e/\tau$ ); (d) the ratios of power factor to the relaxation time ( $PF/\tau$ ) of XY<sub>+</sub>15 GPa at different temperatures.

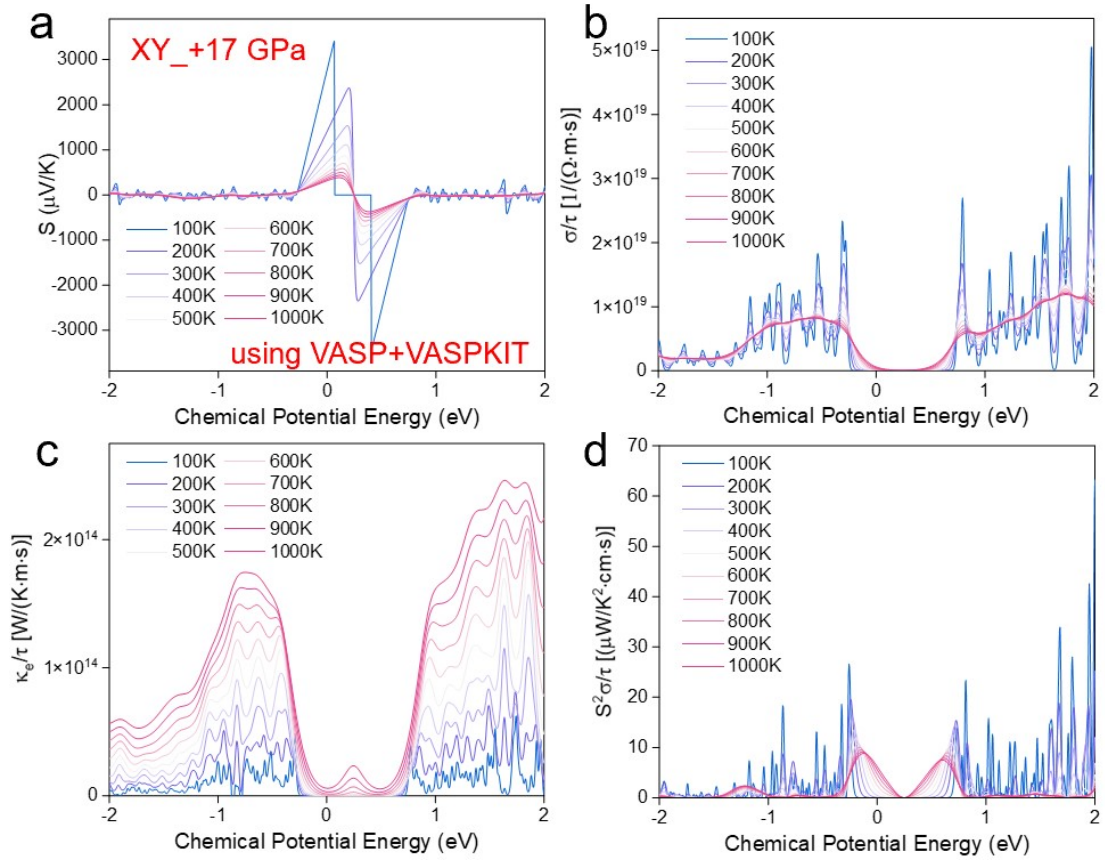


**Fig S22:** The chemical potential-dependent (a) Seebeck coefficient; (b) the ratios of electrical conductivity to the relaxation time ( $\sigma/\tau$ ); (c) the ratios of electronic thermal conductivity to the relaxation time ( $\kappa_e/\tau$ ); (d) the ratios of power factor to the relaxation time ( $PF/\tau$ ) of XY<sub>+</sub>17 GPa at different temperatures.

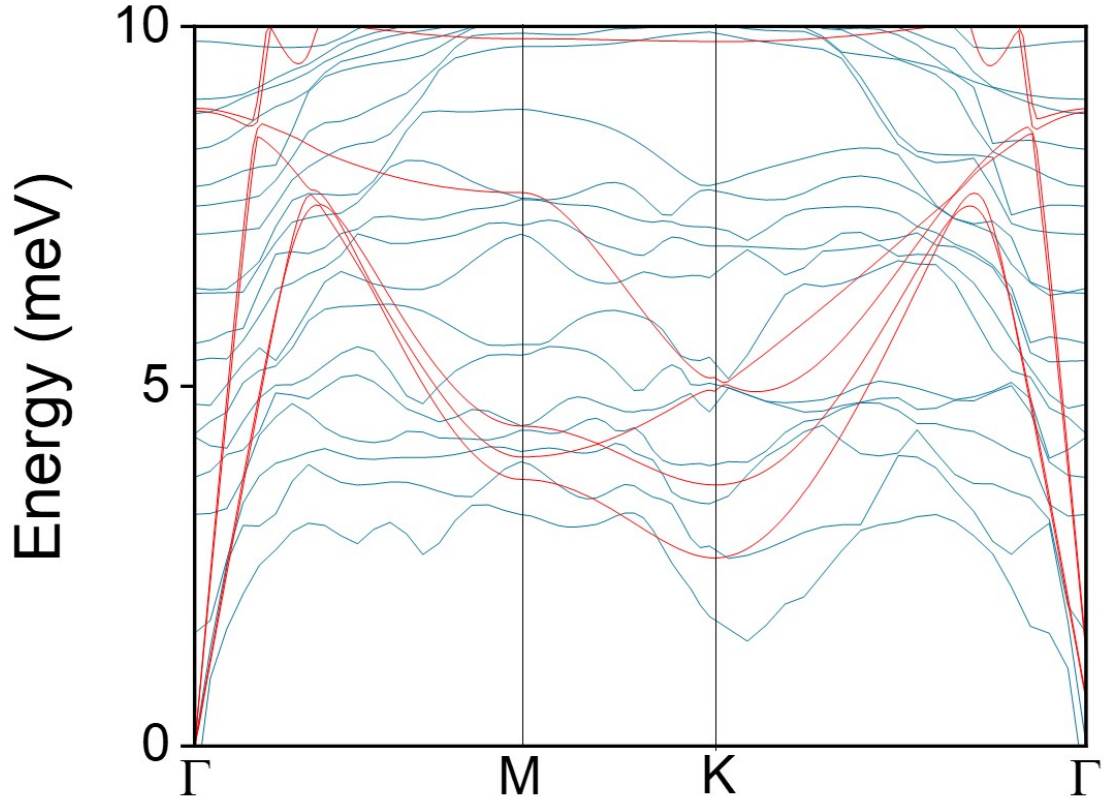


**Fig S23:** The zoomed-in view for both Bilayer and 21.79°\_TBGDY at low frequency, where the blue line represents 21.79°\_TBGDY and the red line represents Bilayer.

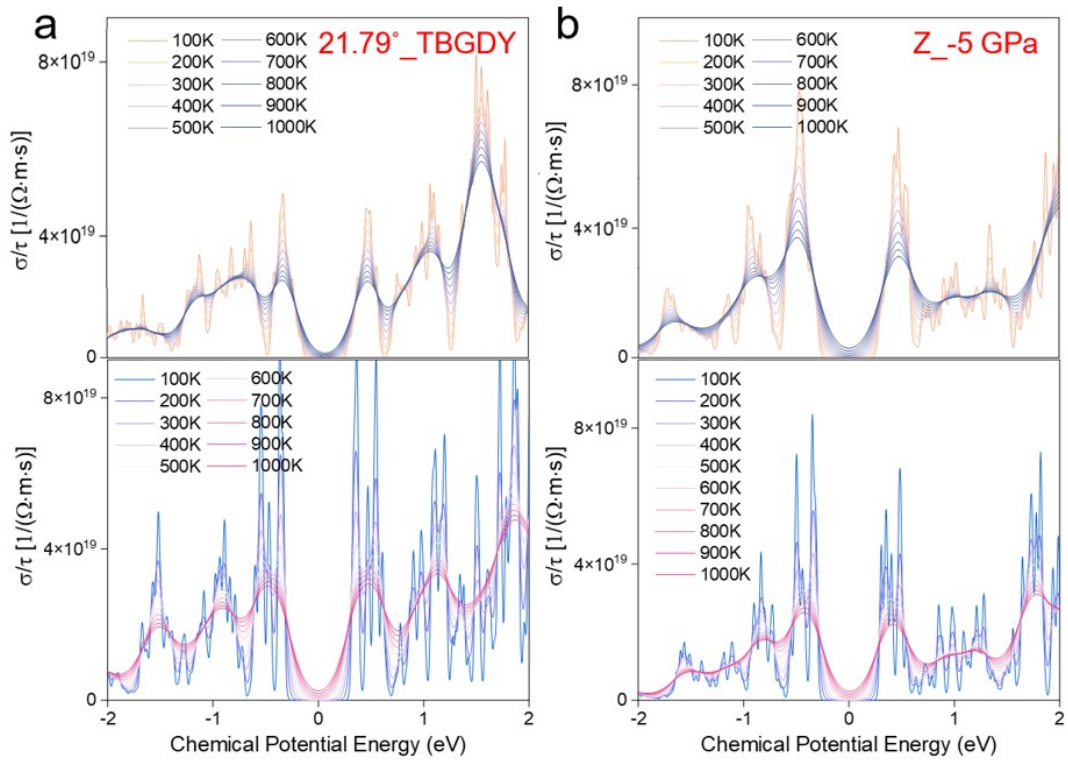


**Fig S24:** (a) Comparison diagram of the ratios of electrical conductivity to the relaxation time ( $\sigma/\tau$ ) of 21.79°\_TBGDY and (b) Z\_-5 GPa calculated. (Two calculation methods: The upper one is the VASP + BoltzTrap method; the lower one is the VASP

+ VASPKIT method).

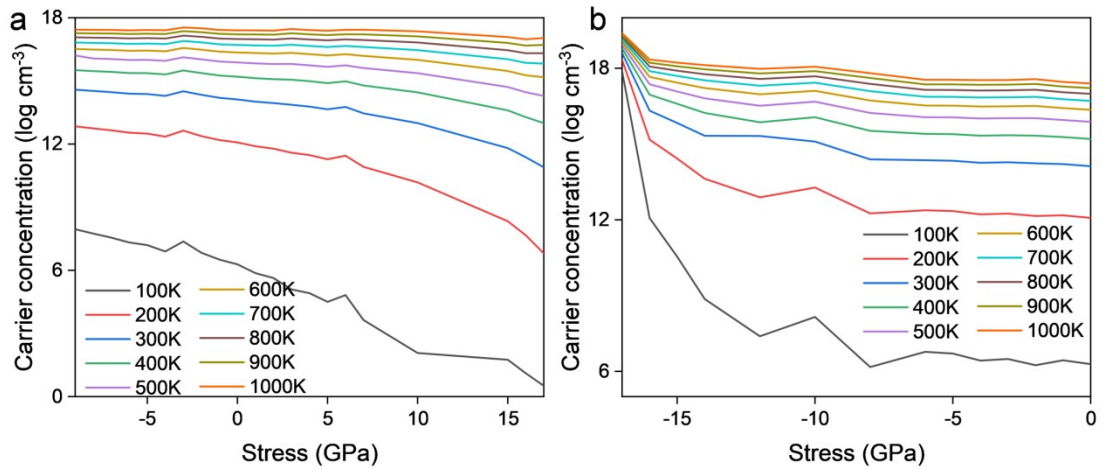


**Fig S25:** (a) Schematic diagram of the carrier concentration of 21.79°\_TBGDY when stress is applied in the in-plane direction (XY direction) at different temperatures (100 ~ 1000K); (b) Schematic diagram of the carrier concentration of 21.79°\_TBGDY when stress is applied in the out-of-plane direction (Z direction) at different temperatures (100 ~ 1000K).